

**Low-Bandgap Dimeric Porphyrin for 10% Efficiency Solar Cells with Small Photon Energy Loss**

Journal:	<i>Journal of Materials Chemistry A</i>
Manuscript ID	TA-ART-06-2018-005903.R1
Article Type:	Paper
Date Submitted by the Author:	19-Jul-2018
Complete List of Authors:	xiao, liangang; South China University of Technology, Lai, Tianqi; South China University of Technology Liu, Xiang; South China Normal University, School of Chemistry and Environment Liu, Feng; Shanghai Jiao Tong University Russell, Thomas; University of Massachusetts, Polymer Science and Engineering Department Liu, Yi; Lawrence Berkeley National Laboratory, The Molecular Foundry Huang, Fei; Institute of Polymer Optoelectronic Materials & Devices, Peng, Xiaobin; South China University of Technology, Cao, Yong; South China University of Technology

A Low-Bandgap Dimeric Porphyrin Molecule for 10% Efficiency Solar Cells with Small Photon Energy Loss

Liangang Xiao,^a Tianqi Lai,^a Xiang Liu,^a Feng Liu^c, Thomas P. Russell^{d,e}, Yi Liu^{b,},
Fei Huang^{a,*}, Xiaobin Peng^{a,*} and Yong Cao^a*

^a Institute of Polymer Optoelectronic Materials and Devices, State Key Laboratory of Luminescent Materials and Devices, South China University of Technology, 381 Wushan Road, Guangzhou 510640, China

Email: F.H: msfhuang@scut.edu.cn; X.P: chxbpeng@scut.edu.cn

^b The Molecular Foundry, Lawrence Berkeley National Laboratory, Berkeley, California 94720, United States

E-mail: yliu@lbl.gov

^c Department of Physics and Astronomy, and Collaborative Innovation Center of IFSA (CICIFSA), Shanghai Jiaotong University, Shanghai 200240, P. R. China

^d Materials Sciences Division, Lawrence Berkeley National Lab, Berkeley, California 94720, United States

^e Polymer Science and Engineering Department, University of Massachusetts, Amherst, Massachusetts 01003, United States

Abstract: Dimeric porphyrin molecules have great potential as donor materials for high performance bulk heterojunction organic solar cells (OSCs). Recently reported

dimeric porphyrins bridged by ethynylenes showed power conversion efficiencies (PCEs) of more than 8%. In this study, we design and synthesize a new conjugated dimeric D-A porphyrin ZnP2BT-RH, in which the two porphyrin units are linked by an electron accepting benzothiadiazole (BT) unit. The introduction of BT unit enhances the electron delocalization, resulting in a lower highest occupied molecular orbital (HOMO) energy level and an increased molar extinction coefficient at the near-infrared (NIR) region. The bulk heterojunction solar cells with ZnP2BT-RH as the donor material exhibit a high PCE up to 10% with a low energy loss (E_{loss}) of only 0.56 eV. The 10% PCE is the highest for porphyrin-based OSCs with a conventional structure, and this E_{loss} is also the smallest among the small molecule-based OSCs with a PCE higher than 10% to date.

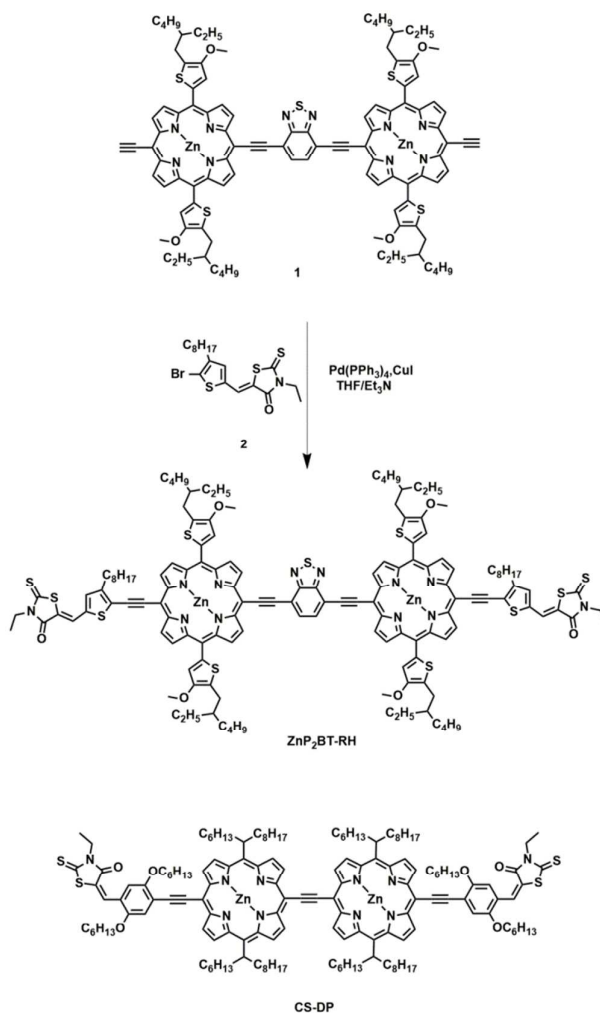
Introduction

In addition to the bulk heterojunction (BHJ) organic solar cells (OSCs) based on polymers,¹⁻⁸ those based on small molecules (SMs) have also attracted much attention due to advantages such as defined molecular structures, reproducible synthesis and less batch-to-batch variations in cell performance.^{9,10} Furthermore, the shorter molecular lengths of SMs result in lower entropic barriers and eliminate the chain entanglements,¹¹ thereby increasing the molecular packing and aggregation in the solid state, which can improve the inter-chain charge transportation. Therefore, power conversion efficiencies (PCEs) comparable to polymer solar cells have been reported for SM solar cells.¹²⁻¹⁴

The PCE of a solar cell is determined by its open circuit voltage (V_{OC}), short circuit current (J_{SC}) and fill factor (FF). In order to improve the J_{SC} , one of the strategies is to reduce the bandgap (E_g) of an active material to absorb more light in a broader wavelength range. However, the reduction of E_g is often accompanied by a V_{OC} decrease. The energy loss (E_{loss}), defined as $E_{loss} = E_g - eV_{OC}$, is thus an important parameter in the evaluation of the solar cell performance.¹⁵⁻¹⁷ The E_{loss} values of inorganic crystalline solar cells are typically $\sim 0.34-0.48$ eV and those of efficient perovskite solar cells are also < 0.5 eV.¹⁸⁻²⁰ However, most OSCs suffer from high E_{loss} values of up to 0.7-0.8 eV, and the quantum efficiencies often drop dramatically when $E_{loss} < 0.6$ eV.²¹⁻²⁴ Therefore, to achieve high PCEs, donor materials with low E_{loss} values that retain high J_{SC} values are highly desired.

Inspired by photosynthesis which utilizes chlorophylls as strong chromophores, porphyrin analogues have been explored as the active materials for organic solar cells, and PCEs up to 9% have been achieved recently.²⁵⁻⁴⁰ Notably, some porphyrin-based OSCs show low E_{loss} values with high J_{SC} values. To further increase the J_{SC} values and therefore the PCEs of porphyrin-based OSCs, we developed a series of porphyrin dimers, where porphyrin units were bridged by electron-rich ethynylene, diethynylene, diethynylenedithiophene or diethynylene-phenylene linkers, since extending the molecular conjugation length in oligoporphyrins was reported to be effective in increasing the molar coefficient and extending the absorption wavelength range.⁴¹⁻⁴⁶ However, the highest PCE was only 8% for the dimeric porphyrin-based OSCs.⁴⁷⁻⁴⁹

Considering that alternating electron donor–acceptor (D-A) units in molecular structures can enhance the π electron delocalization and improve the light extinction coefficient due to intramolecular charge transfer,⁵⁰⁻⁵⁴ we incorporate an electron acceptor unit between the two porphyrin units, and design and synthesize an A1-D-A2-D-A1 type dimeric porphyrin ZnP2BT-RH by appending 2-methylene-3-ethylrhodanine (RH) end units (A1) via ethynylene linkages to two porphyrin donor units (D) bridged by another electron acceptor unit (A2) benzothiadiazole (BT) (Scheme 1). ZnP2BT-RH shows an enhanced molar extinction coefficient of the NIR absorption peak, larger than previously reported porphyrin dimers without central electron-withdrawing unit. Furthermore, the electron-withdrawing BT unit can down-shift the highest occupied molecular orbital energy level (E_{HOMO}), thus increasing the gap between the E_{HOMO} of the donor and the lowest unoccupied molecular orbital energy level (E_{LUMO}) of PC₇₁BM. A high V_{OC} of 0.845 V, a J_{SC} of 17.66 mA cm⁻², a FF of 67.15% and a PCE up to 10.02% are achieved for the corresponding devices with an E_{loss} of only 0.56 eV. The 10% PCE is the highest reported for porphyrin-based OSCs with a conventional structure, and the E_{loss} is also the smallest among the small molecule-based OSCs with a PCE higher than 10% to date.



Scheme 1. The synthetic route of ZnP₂BT-RH and chemical structure of CS-DP.

Experimental section

Materials. All reagents were purchased from commercial sources (Aldrich, Acros, Energy chemical or Suna Tech Inc.) and used as received. Tetrahydrofuran (THF) and toluene were dried over Na/benzophenoneketyl and freshly distilled prior to use. Experiments details, ¹H NMR, MALDI-TOF and UV-vis-NIR spectra for the molecule, optimal photovoltaic properties, and mobility measurement, AFM, thermogravimetric analysis (TGA) and GIXD of pure porphyrin are available in the support information.

ZnP2BT-RH: Compound **1** (187mg, 0.10 mmol) was dissolved in THF (20 mL) and triethylamine (10 mL) with compound **2** (0.30 mmol). Then Pd(PPh₃)₄ (12 mg, 0.01mmol) and CuI (2 mg, 0.01mmol) were added. After the mixture was stirred at 60 °C for 48 h under argon, the reaction was quenched with saturated brine. After the mixture was extracted with chloroform, dried with anhydrous Na₂SO₄ and the concentrated, the residue was column chromatographed on silica gel using CH₂Cl₂ as eluent to give a black solid of ZnP2BT-RH. (170 mg, 65% yield).

ZnP2BT-RH: ¹HNMR (500 MHz, CDCl₃) δ/ppm (ppm): ¹HNMR (500 MHz, CDCl₃) δ/ppm (ppm): 10.66-9.60 (m, 16H), 8.58-7.73 (m, 12H), 7.58 (s, 4H), 6.45(s, 2H), 4.36 (s, 12H), 3.64-3.27 (m, 8H), 2.45-2.15 (m, 4H), 2.15-1.04 (m, 86H), 0.91 (s, 6H). MALDI-TOF Mass (m/z): calculated for C₁₄₂H₁₅₀N₁₂O₆S₁₁Zn₂: 2601.73; found: 2602.25. UV-vis (THF), λ_{max}=508 nm.

Results and Discussion

The synthesis of the dimeric porphyrin small molecule ZnP2BT-RH is shown in Scheme 1 and Scheme S1. ZnP2BT-RH is a black solid with good thermal stability (SI) and enough solubility in common organic solvents such as chloroform (CF), tetrahydrofuran (THF) and toluene, and its chemical structure is confirmed by NMR spectroscopy (Figure S1) and matrix-assisted laser desorption/ionization time-of light (MALDI-TOF) mass spectrometry (Figure S2). The ultraviolet-visible-near-infrared

(UV-vis-NIR) absorption spectrum of ZnP2BT-RH in THF shows two absorption bands (Figure 1a) at 510 (Soret band) and 761 nm (Q band) with almost the same molar extinction coefficient (ϵ) of $2.24 \times 10^5 \text{ M}^{-1} \text{ cm}^{-1}$ (Figure S3). Since the Soret band can be ascribed to the $\pi-\pi^*$ transition of the conjugated backbone and the Q band in the region of 700-850 nm is attributable to the intramolecular charge transfer (ICT) band,⁵⁵ the increased ϵ of the Q band indicates a more efficient ICT in ZnP2BT-RH than that in CS-DP (Scheme 1 and Figure S3, the ϵ of Q band: $1.28 \times 10^5 \text{ M}^{-1} \text{ cm}^{-1}$).⁴⁸

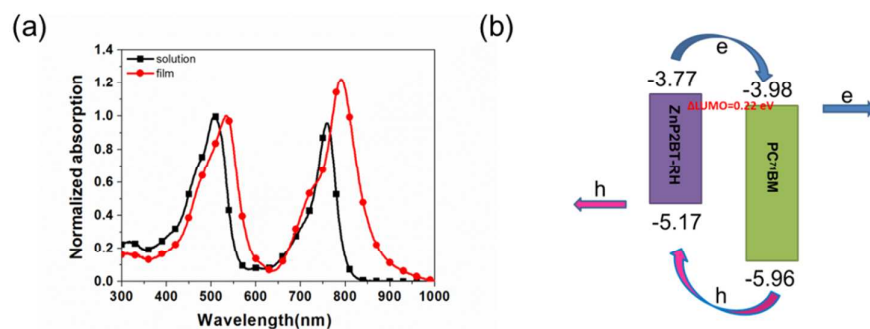


Figure 1. a) Normalized UV-vis-NIR absorption spectra of ZnP2BT-RH in solution (THF) and in film; b) the energy level diagram of ZnP2BT-RH and PC₇₁BM.

Compared with the absorption spectrum in solution, ZnP2BT-RH films show significantly red-shifted peaks with an onset at 885 nm, from which the optical band gap ($E_{g(\text{opt})}$) is calculated to be 1.40 eV. To estimate the E_{HOMO} and E_{LUMO} , we measure the cyclic voltammetry (CV) of ZnP2BT-RH under an inert atmosphere in acetonitrile using tetrabutylammonium hexafluorophosphate (Bu_4NPF_6 , 0.10 M) as the supporting electrolyte, a glassy carbon working electrode, a platinum wire counter electrode and an Ag/AgCl reference electrode. As shown in Table 1 and Figure S4,

the onset oxidation potential (E_{ox}) of ZnP2BT-RH is 0.77 V vs. Fc/Fc⁺, from which the E_{HOMO} is estimated to be -5.17 eV from $E_{\text{HOMO}} = -(E_{\text{ox}} + 4.4)$ eV, and the E_{LUMO} is -3.77 eV according to $E_{\text{LUMO}} = E_{\text{HOMO}} + E_{\text{g(opt)}}$. Compared with the E_{HOMO} (-4.96 eV) and E_{LUMO} (-3.74 eV) of CS-DP, the E_{HOMO} is notably reduced while the E_{LUMO} is quite similar.

Table 1. The optical and electrochemical data of ZnP2BT-RH

$\lambda_{\text{max}}/\text{nm}$ (solution)	$\lambda_{\text{max}}/\text{nm}$ (film)	$\lambda_{\text{onset}}/\text{nm}$ (film)	E_{ox} [V]	E_{HOMO}^a [eV]	E_{LUMO}^b [eV]	$E_{\text{g(opt)}}$ [eV]
507, 761	535, 792	885	0.77	-5.17	-3.77	1.40

^a $E_{\text{HOMO}} = -e (E_{\text{ox}} + 4.4)$ V; ^b $E_{\text{LUMO}} = E_{\text{HOMO}} + E_{\text{g(opt)}}$.

To evaluate the photovoltaic performance of ZnP2BT-RH-based solar cells, solution-processed BHJ OSCs are fabricated using ZnP2BT-RH as the electron donor and [6,6]-phenyl C₇₁-butyric acid methyl ester (PC₇₁BM) as the electron acceptor with a conventional device structure of ITO/PEDOT:PSS/active layer/PNDIT-F3N-Br/Al (ITO: indium tin oxide, PEDOT:PSS: poly(styrene sulfonate)-doped poly(ethylene-dioxythiophene), PNDIT-F3N-Br: poly[(9,9-bis(3'-((N,N-dimethyl)-N-ethylammonium)propyl)-2,7-fluorene)-alt-5,5'-bis(2,2'-thiophene)-2,6-naphthalene-1,4,5,8-tetracarboxylic-N,N'-di(2-ethylhexyl)imide] dibromide.⁵⁶ The current density (J)–voltage (V) curves of the ZnP2BT-RH-based OSCs are shown in Figure 2a and Figure S5-S6 with the photovoltaic parameters summarized in Table 2 and Table S1-S3. The donor-acceptor weight ratio is optimized to be 1:1.5, and the thickness of the active layer is ~110 nm. The solar cells

based on as-cast ZnP2BT-RH/PC₇₁BM films shows a PCE of 5.23% with a high V_{oc} of 0.91 V. While thermal annealing (TA) of the blend films at 135°C only slightly improved the efficiency to 5.68%, further chloroform solvent vapor annealing (SVA) (namely TA+SVA) dramatically enhances the efficiency to 9.00% with a slightly reduced V_{oc} of 0.84 V but significantly increased J_{sc} and FF values of 16.49 mA cm⁻² and 63.87%, respectively. Though the FF is smaller than those of CS-DP-based devices (69.80%), this PCE is higher than that of CS-DP-based devices (8.29%) due to the improved J_{sc} and V_{oc} , which can arise from the deeper E_{HOMO} and enhanced ICT in ZnP2BT-RH with the introduction of the electron withdrawing BT unit.

Surprisingly, in contrast to early reported OSCs based on monomeric porphyrins and other small molecules,⁵⁷⁻⁵⁹ the performance of the devices with only SVA is superior to those with TA + SVA. With chloroform SVA for 240 s, the PCE reaches 10.02% with a J_{sc} of 17.66 mA cm⁻², a V_{oc} of 0.845 V, and a FF of 67.15%. The 10% PCE is the highest for porphyrin-based OSCs using a conventional structure to date. Furthermore, the efficiencies remain above 9% for different SVA times from 220 to 280 s. However, further TA after SVA (SVA+TA) reduces the device performance significantly with PCE, J_{sc} and FF values of only 7.60%, 15.79 mA cm⁻² and 55.97%, respectively. It is noted that the V_{oc} values still remain high (0.84–0.91 V) while the J_{sc} and FF values change dramatically under the different processing conditions. From the optical bandgap and the V_{oc} values, the E_{loss} values of the devices are calculated to be 0.49–0.56 eV. The E_{loss} of 0.56 eV is the smallest for small-molecule OSCs with PCE >10%¹²⁻¹⁴ and also one of the smallest for

organic solar cells with PCE over 9% (Table S4).^{1, 60-65} One of the reasons why the devices based on ZnP2BT-RH show such low E_{loss} values can be the relatively high dielectric constant of ZnP2BT-RH (4.07 at 10 kHz) in comparison to those of previously reported porphyrin derivatives DPPEZnP-TEH (3.90 at 10 kHz) and those of other well-known OSC donors (Figure S7), since the higher dielectric constant facilitates charge separation and contributes to a lower E_{loss} .²³

Table 2. The photovoltaic parameters of ZnP2BT-RH-based solar cells under different process conditions.

Conditions	J_{SC} (mA cm ⁻²)	V_{OC} (V)	FF (%)	PCE(%)
CAST	13.31±0.21	0.91±0.004	42.34±0.65	5.13±0.23 ^b (5.23) ^a
TA	14.15±0.33	0.91±0.005	42.85±0.63	5.52±0.28 ^b (5.68) ^a
TA+SVA	16.49±0.24	0.84±0.005	63.87±0.47	8.85±0.23 ^b (9.00) ^a
SVA	17.49±0.24	0.84±0.005	66.79±0.55	9.81±0.24 ^b (10.02) ^a
SVA+TA	15.79±0.31	0.86±0.010	55.97±0.66	7.60±0.37 ^b (7.83) ^a

^a The best PCE; ^b average PCE of 20 devices.

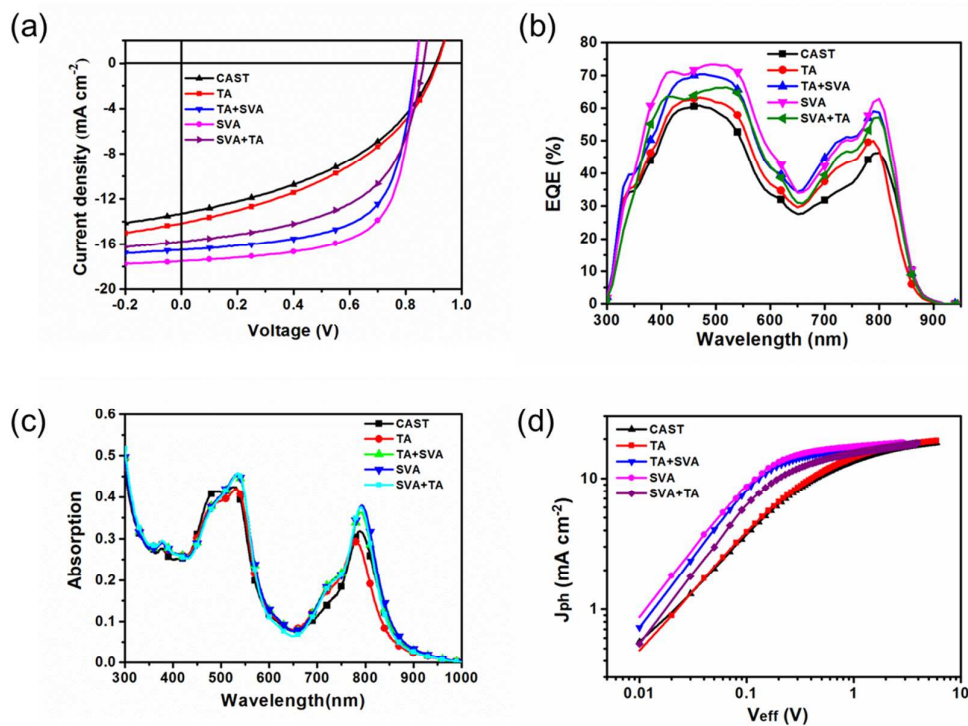


Figure 2. a) $J-V$ curves, b) EQE curves of ZnP2BT-RH-based solar cells, c) the absorption spectra of ZnP2BT-RH/PC₇₁BM blend films, and d) photocurrent density versus effective voltage curves of ZnP2BT-RH based solar cells under the different processing conditions.

The external quantum efficiency (EQE) curves are measured to explore the spectral response of the devices fabricated with the three different post-treatments. As shown in Figure 2b, the devices convert photons into electrons efficiently over the wavelength range of 300-800 nm, and lower EQEs tailing to 900 nm. While the as-cast devices show EQE peaks at 470 and 800 nm with high EQE values of 61% and 46%, respectively, TA at 135°C slightly increases the EQE values between 300 and 800 nm with a marginally blue-shifted photo response. The EQE peak in the NIR region ($\sim 790 \text{ nm}$) is 50%. In line with the significantly enhanced J_{SC} values, the

devices with TA+SVA show improved EQE values from 300 to 900 nm, and the highest EQEs are observed for SVA-only devices with EQEs over 70% between 410 and 540 nm. The calculated J_{SC} from the EQE measurement is 16.92 mA cm^{-2} , which is slightly lower but within 5% errors compared to the J_{SC} obtained from the $J-V$ measurements. Further TA (SVA+TA) reduces the photo-to-electric response in the whole wavelength region in comparison to the SVA-only devices. The high EQE values imply a low binding energy of the excitons though the E_{LUMO} difference of ZnP2BT-RH and PC₇₁BM (ΔE_{LUMO}) is smaller than the empirical threshold of 0.3 eV (energy level diagram was shown in Figure 1b).

To investigate the molecular aggregation behavior, the absorption spectra of the blend films with the different post-treatments are measured and shown in Figure 2c. While the NIR absorption peak of the as-cast blend film is at 788 nm, that of the TA treated ones is blue-shifted to 780 nm with a decreased intensity. SVA, TA+SVA and SVA+TA post-treatments red-shift the NIR peaks with enhanced absorption intensities. In addition, a slight yet noticeable blue-shift can be observed for the SVA+TA blends in comparison to the absorption of SVA samples, which is similar to the absorption changes when the as-cast blend is thermally annealed, indicating the different aggregation behavior induced by TA and SVA.

We measure the current density-voltage characteristics in the dark under reverse and forward biases (Figure S8) to investigate the rectification behavior of the as-cast devices and the devices with SVA and SVA+TA. In comparison to the as-cast devices, the SVA treated devices show higher current density under forward bias but smaller

dark current density under reverse bias, leading to an enhanced rectification ratio of 5.04×10^5 versus 7.54×10^4 for as-cast devices at ± 2 V. Upon further TA (SVA+TA), the forward current densities decrease while the reverse ones increase, reducing the diode performance. These results suggest that SVA suppresses the leakage current and improve the diode behavior but further TA has an adverse effect, possibly due to the overgrowth of ZnP2BT-RH crystalline phases and the changes of the vertical phase separation.⁶⁶

We also investigate the hole mobilities of ZnP2BT-RH:PC₇₁BM blend films under the different processing conditions using a device structure of ITO/PEDOT:PSS/ZnP2BT-RH:PC₇₁BM/MoO₃/Ag by the SCLC (space-charge limited current) method. As shown in Figure S9 and listed in Table S5, the as-cast blend shows a mobility of $1.21 \times 10^{-5} \text{ cm}^2 \text{ V}^{-1} \text{ s}^{-1}$, and the blend with TA shows a similar mobility of $1.43 \times 10^{-5} \text{ cm}^2 \text{ V}^{-1} \text{ s}^{-1}$. However, the TA+SVA and SVA treated ZnP2BT-RH:PC₇₁BM blends show mobilities up to 3.40×10^{-4} and $4.94 \times 10^{-4} \text{ cm}^2 \text{ V}^{-1} \text{ s}^{-1}$, respectively, more than one order of magnitude higher than those without SVA. These values are also higher than that of CS-DP-based devices with TA+SVA ($1.44 \times 10^{-4} \text{ cm}^2 \text{ V}^{-1} \text{ s}^{-1}$), indicating better charge transport in ZnP2BT-RH-based devices. In line with the FF changes, further TA of the SVA film (SVA+TA) reduced the hole mobility to $1.08 \times 10^{-4} \text{ cm}^2 \text{ V}^{-1} \text{ s}^{-1}$.

To gain insight into exciton dissociation and charge generation of ZnP2BT-RH based solar cells under different processing conditions, we further investigate the relationships between the photocurrent density (J_{ph}) and the effective voltage (V_{eff}) of

the cells (Figure 2d). J_{ph} and V_{eff} are defined by the equations of $J_{\text{ph}}=J_{\text{L}}-J_{\text{D}}$ and $V_{\text{eff}}=V_{\text{o}}-V_{\text{a}}$, where J_{L} and J_{D} are the current densities under illumination and in the dark, respectively, and V_{o} is the voltage at $J_{\text{ph}}=0$ and V_{a} is the applied voltage.⁶⁷ As shown in Figure 2d, the J_{ph} values of the devices with TA+SVA and SVA are markedly higher and almost saturated (J_{sat}) at a relatively lower V_{eff} , indicating more efficient exciton dissociation and carrier collection. The J_{ph} values of the as-cast and TA treated devices, on the other hand, are still not saturated even when V_{eff} is 5 V, an indication of severe charge recombination. It is generally assumed that all the photo-generated excitons are dissociated into free charge carriers when the V_{eff} is high enough. Therefore, the saturation current (J_{sat}) only depends on the maximum exciton generation rate (G_{max}) calculated from $J_{\text{sat}}=qLG_{\text{max}}$, where q is the elementary charge and L is the thickness of the active layer.^{39, 68} The SVA devices show a maximum exciton G_{max} of $1.05 \times 10^{28} \text{ m}^{-3} \text{ s}^{-1}$ ($J_{\text{sat}}=183.9 \text{ A m}^{-2}$) that is higher than that of the devices processed with TA+SVA (G_{max} is $1.01 \times 10^{28} \text{ m}^{-3} \text{ s}^{-1}$ at a J_{sat} of 178.1 A m^{-2}). The increased G_{max} indicates the generation of more excitons, which is consistent with the enhanced absorbance as shown in Figure 2c. It should be noted that the small G_{max} difference cannot fully account for the large PCE difference. Another parameter, $P(\text{E,T})$, determined by $J_{\text{ph}}/J_{\text{sat}}$ under short circuit conditions, should be taken into consideration to indicate the charge collection probabilities. The $P(\text{E,T})$ values for TA+SVA and SVA devices are 92.5% and 95.2%, respectively. The larger G_{max} and $P(\text{E,T})$ values for SVA devices correlate well with the higher J_{SC} and FF. For SVA+TA devices, although the J_{sat} is similar to that of SVA devices, the moderate

$P(E,T)$ of 87.3% suggests inefficient charge separation, leading to a poor FF of 56.19% and a moderate PCE of 7.83%. All these results reveal that SVA is the most efficient in enhancing the charge separation, which simultaneously improves J_{SC} and FF .

The recombination process of these devices is investigated by measuring the J_{SC} values at various light intensities. In principle, J_{SC} shows a power-law dependence on light intensity for organic solar cells, which can be expressed as $J_{SC} \propto (P_{light})^S$ (P_{light} is the light intensity and S is the exponential factor).⁶⁹ When all free charges are swept out and collected at the electrodes prior to recombination, S value should be 1. Figure 3a shows the relationship of J_{SC} against light intensity of the devices under the three different processing conditions, and the S values are calculated to be 0.931, 0.982 and 0.948 for the as-cast, SVA and SVA+TA devices, respectively. The highest S value of the SVA-treated device suggests the most effective suppression of bimolecular recombination, leading to the highest J_{SC} and FF . V_{OC} values are also measured at various light intensities to get a deeper insight into the recombination mechanisms.⁷⁰ Figure 3b shows the relationships between the V_{OC} and the P_{light} of the devices under the three different processing conditions. Generally, a slope of $1 k_B T/q$ implies that bimolecular recombination is the dominating mechanism (k_B is Boltzmann's constant, T is temperature and q is elementary charge), while a dependence of V_{oc} on light intensity with a slope of $2 k_B T/q$ would be observed for trap-assisted or monomolecular recombination.^{71,72} The slope of $1.20 k_B T/q$ for the ZnP2BT-RH-based devices without any post-treatment implies that the bimolecular

recombination is dominant, possibly due to the good mixing of ZnP2BT-RH with PC₇₁BM, which provide sufficient interfaces for exciton separation but non-ideal crystallinity for efficient charge transport, leading to severe bimolecular recombination between the holes and electrons. On the other hand, the SVA and SVA+TA treated devices show slopes of 1.45 and 1.54 $k_B T/q$, respectively, suggesting that the bimolecular recombination can be significantly suppressed by SVA.

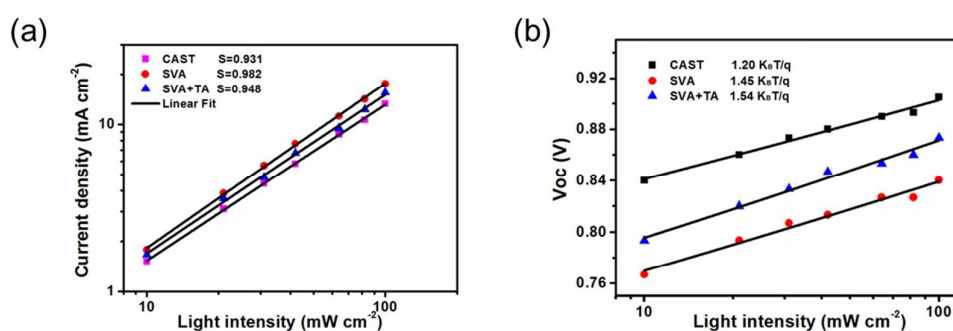


Figure 3. Dependence of (a) J_{sc} and (b) V_{oc} on light intensity for the ZnP2BT-RH based solar cells under the three processing conditions.

We also investigate the morphology of ZnP2BT-RH:PC₇₁BM active layers under the different processing conditions, using atomic force microscopy (AFM), grazing incidence X-ray diffraction (GIXD) and resonant soft X-ray scattering (RSoXS). As shown in Figure S10, the root-means-square (RMS) roughness values of the as-cast and SVA treated films are less than 1 nm, and the TA+ SVA treated films show a slightly increased RMS of 1.5 nm. GIXD profiles of the pure ZnP2BT-RH films and blend films under different processing conditions show more details of the intrinsic ordering of the components, as shown in Figure 4 and Figure S11. For the

ZnP2BT-RH samples spin-coated from pure THF solution, a sharp peak at 0.28 \AA^{-1} is observed in the low q region, attributable to the lamellar stacking in the (100) direction. The crystalline nature of ZnP2BT-RH becomes less pronounced when pyridine is used as an additive, as supported by the increased peak width, reduced peak intensity at 0.28 \AA^{-1} and the disappearance of the peaks at 0.57 \AA^{-1} (200) and 0.85 \AA^{-1} (300) in the out-of-plane GIXD pattern. For TA or SVA films, higher order peaks at (200) and (300) reappear, indicating that TA and SVA promote the crystallization. In comparison to other samples, the d spacing of the (100) reflection of the SVA sample decreases slightly, in accordance with a tighter lamellar packing that is conducive to carrier transport. Furthermore, the π - π stacking peak at 1.86 \AA^{-1} is observed after TA or SVA treatment. The similar crystallinity of TA, TA+SVA and SVA+TA samples arises from the fact that the porphyrin crystallinity can be fixed after TA and is hard to change with further SVA. Therefore, the effects of TA on crystallization are greater than those of SVA. Subsequent TA to SVA-treated film can endow crystallinity similar to TA-only film. For the blend samples, the as-cast films show a weak π - π stacking reflection in the in-plane direction, indicating a weak edge-on crystal orientation. Diffuse Bragg rods are also observed in the in-plane direction. These features arise from the self-assembly of ZnP2BT-RH molecules into thin layers in the donor domains.⁴⁸ The TA and SVA films show a quite broad, azimuthally-independent (100) diffraction reflection at 0.28 \AA^{-1} (2.24 nm), indicating that there is no preferred crystal orientation and the transformation of crystals from edge-on to face-on. In addition, a broad reflection from PC₇₁BM is seen at 1.31 \AA^{-1} .

Importantly, for the TA, TA+SVA, SVA or SVA+TA films, a π - π stacking peak (due to ZnP2BT-RH) can be seen at 1.86 \AA^{-1} (0.34 nm), which correlates with the improved J_{SC} values. In addition, the peak areas of the films with TA+SVA and SVA are slightly larger than those of the TA and SVA+TA treated films, suggesting better crystallinity in TA+SVA and SVA treated films and are consistent with their better device performance.

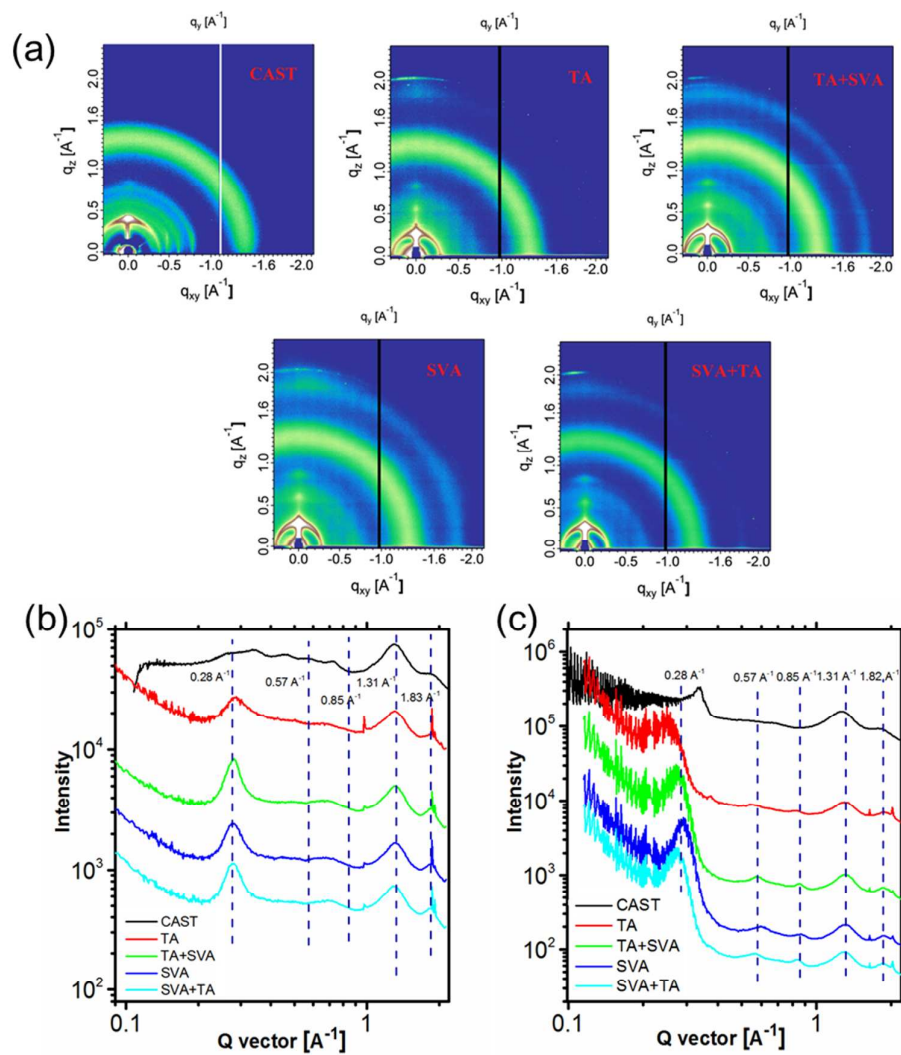


Figure 4. Grazing incidence X-ray diffraction (GIXD) patterns (a), in-plane (b) and out-of-plane (c) line-cut profiles of BHJ thin films

The phase separation of these blend films is studied using resonant soft X-ray scattering (RSoXS) by taking advantage of the high optical contrast at the carbon K-edge (284.2 eV). Shown in Figure 5 are the scattering profiles of the five blend films under the different processing conditions. The as-cast films show very low scattering intensities and no obvious interferences, suggesting a lack of phase separation due to the miscibility of ZnP2BT-RH and PC₇₁BM that is mediated by pyridine. This is consistent with previous works that strong recombination is commonly observed for well-mixed systems.^{27, 72} For the TA-treated blend film, a plateau in the scattering is seen at $\sim 0.022 \text{ \AA}^{-1}$, corresponding to a domain size of 28.6 nm. The low scattering intensity indicates a weak degree of phase separation, and thus, the TA devices show an only slightly improved J_{SC} in comparison to the as-cast films. The SVA of the TA film leads to significantly enhanced scattering over the entire q region and an obvious peak is observed at 0.016 \AA^{-1} , corresponding to a distance of 39.2 nm. The significantly increased scattering intensity suggests the enhanced phase separation, which correlates well with the increase in the PCE from 5.68% to 9.00%. For the SVA film, the phase separated domain size (44.8 nm) is slightly larger than that of the TA+SVA film, which is beneficial for more balanced exciton separation and charge transportation. Furthermore, the SVA film also has better phase purity. These collective morphological features correlate well with the champion devices from solvent vapor annealing. However, for the SVA +TA film, a sharp upturn in the scattering at very low q is observed, consistent with an increase in

the surface roughness and the device performance. Other factors like the diffusion of PC₇₁BM to the layer of PEDOT:PSS and vertical phase separation change after TA treatment was not observed contributing to the decrease in performance.

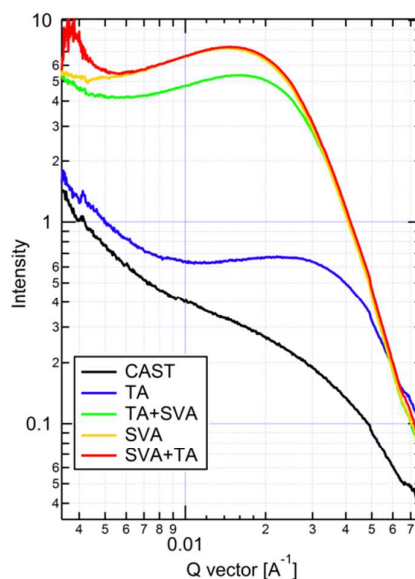


Figure 5. Resonant soft X-ray scattering (RSoXS) profiles of BJJ thin films.

Conclusion

In summary, a dimeric porphyrin small molecule ZnP2BT-RH, where the two porphyrin units are linked with the electron withdrawing unit BT, has been developed for OSCs. The introduction of BT not only enhances the π electron delocalization to improve the intramolecular charge transfer and the molar extinction coefficient of the NIR absorption band but also downshifts the HOMO energy level, which are beneficial for the V_{OC} enhancement without sacrificing J_{SC} for ZnP2BT-RH-based OSCs. SVA treatment induces π - π stacking and tightens lamellar packing, which benefits carrier transportation. Phase separation and improved phase purity of the

SVA-treated films greatly enhance the exciton separation and carrier collection efficiency and reduce the recombination. After optimizing the processing conditions, excellent device performance with PCEs up to 10.02% is achieved with a low E_{loss} of only 0.56 eV, which is the smallest E_{loss} to date for small molecule-based OSCs with PCEs more than 10%. The 10% PCE is the highest for porphyrin-based BHJ solar cells and also ranks one of the highest small molecule solar cells.

Conflicts of interest

The authors declare no competing financial interest.

Acknowledgements

This work was financially supported by the grants from the National Natural Science Foundation of China (51773065 and 51473053), the National Key Research and Development Program of China (2017YFA0206602), International Science and Technology Cooperation Program of China (2013DFG52740), and the Fundamental Research Funds for the Central Universities. TPR were supported by the U.S. Office of Naval Research under contract N00014-15-1-2244. Portions of this research were carried out as a user project at the Molecular Foundry, and the X-ray experiments were carried out at beamline 7.3.3 and 11.0.1.2 at the Advanced Light Source, Lawrence Berkeley National Laboratory, all supported by the Office of Science, Office of Basic Energy Sciences, of the U. S. Department of Energy under Contract No. DE-AC02-05CH11231.

References

1. P. Cheng, M. Y. Zhang, T. K. Lau, Y. Wu, B. Y. Jia, J. Y. Wang, C. Q. Yan, M. Qin, X. H. Lu and X. W. Zhan, *Adv. Mater.*, 2017, **29**, 1605216-1605221.
2. J. D. Chen, C. H. Cui, Y. Q. Li, L. Zhou, Q. D. Ou, C. Li, Y. F. Li and J. X. Tang, *Adv. Mater.*, 2015, **27**, 1035-1041.
3. X. H. Ouyang, R. X. Peng, L. Ai, X. Y. Zhang and Z. Y. Ge, *Nat. Photonics*, 2015, **9**, 520-525.
4. N. L. Qiu, H. J. Zhang, X. J. Wan, C. X. Li, X. Ke, H. R. Feng, B. Kan, H. T. Zhang, Q. Zhang, Y. Lu and Y. S. Chen, *Adv. Mater.*, 2017, **29**, 1604964-1604968.
5. S. S. Li, L. Ye, W. C. Zhao, S. Q. Zhang, S. Mukherjee, H. Ade and J. H. Hou, *Adv. Mater.*, 2016, **28**, 9423-9429.
6. Z. C. He, B. Xiao, F. Liu, H. B. Wu, Y. L. Yang, S. Xiao, C. Wang, T. P. Russell and Y. Cao, *Nat. Photonics*, 2015, **9**, 174-179.
7. Y. H. Liu, J. B. Zhao, Z. K. Li, C. Mu, W. Ma, H. W. Hu, K. Jiang, H. R. Lin, H. Ade and H. Yan, *Nat. Commun.*, 2014, **5**, 5293-5300.
8. W. C. Zhao, S. S. Li, H. F. Yao, S. Q. Zhang, Y. Zhang, B. Yang and J. H. Hou, *J. Am. Chem. Soc.*, 2017, **139**, 7148-7151.
9. J. L. Wang, K. K. Liu, J. Yan, Z. Wu, F. Liu, F. Xiao, Z. F. Chang, H. B. Wu, Y. Cao and T. P. Russell, *J. Am. Chem. Soc.*, 2016, **138**, 7687-7697.
10. L. G. Xiao, S. Chen, X. B. Chen, X. B. Peng, Y. Cao and X. J. Zhu, *J. Mater. Chem. C.*, 2018, **6**, 3341-3345.
11. L. Zhang, F. Liu, Y. Diao, H. S. Marsh, N. S. Colella, A. Jayaraman, T. P. Russell, S. C. B. Mannsfeld and A. L. Briseno, *J. Am. Chem. Soc.*, 2014, **136**, 18120-18130.
12. B. Kan, M. M. Li, Q. Zhang, F. Liu, X. J. Wan, Y. C. Wang, W. Ni, G. K. Long, X. Yang, H. R. Feng, Y. Zuo, M. T. Zhang, F. Huang, Y. Cao, T. P. Russell and Y. S. Chen, *J. Am. Chem. Soc.*, 2015, **137**, 3886-3893.
13. D. Deng, Y. J. Zhang, J. Q. Zhang, Z. Y. Wang, L. Y. Zhu, J. Fang, B. Z. Xia, Z. Wang, K. Lu, W. Ma and Z. X. Wei, *Nat. Commun.*, 2016, **7**, 13740-13748.
14. J. Wan, X. Xu, G. Zhang, Y. Li, K. Feng and Q. Peng, *Energy Environ. Sci.*, 2017, **10**, 1739-1745.
15. R. A. J. Janssen and J. Nelson, *Adv. Mater.*, 2013, **25**, 1847-1858.
16. D. Veldman, S. C. J. Meskers and R. A. J. Janssen, *Adv. Funct. Mater.*, 2009, **19**, 1939-1948.
17. K. Gao, L. G. Xiao, Y. Y. Kan, B. L. Yang, J. B. Peng, Y. Cao, F. Liu, T. P. Russell and X. B. Peng, *J. Mater. Chem. C.*, 2016, **4**, 3843-3850.
18. D. Q. Bi, C. Y. Yi, J. S. Luo, J. D. Decoppet, F. Zhang, S. M. Zakeeruddin, X. Li, A. Hagfeldt and M. Gratzel, *Nat. Energy*, 2016, **1**, 1-5.
19. P. K. Nayak and D. Cahen, *Adv. Mater.*, 2014, **26**, 1622-1628.
20. M. Saliba, T. Matsui, K. Domanski, J. Y. Seo, A. Ummadisingu, S. M. Zakeeruddin, J. P. Correa-Baena, W. R. Tress, A. Abate, A. Hagfeldt and M. Gratzel, *Science*, 2016, **354**, 206-209.
21. W. W. Li, K. H. Hendriks, A. Furlan, M. M. Wienk and R. A. J. Janssen, *J. Am. Chem. Soc.*, 2015, **137**, 2231-2234.
22. M. Wang, H. B. Wang, T. Yokoyama, X. F. Liu, Y. Huang, Y. Zhang, T. Q. Nguyen, S.

- Aramaki and G. C. Bazan, *J. Am. Chem. Soc.*, 2014, **136**, 12576-12579.
23. K. Gao, L. S. Li, T. Q. Lai, L. G. Xiao, Y. Huang, F. Huang, J. B. Peng, Y. Cao, F. Liu, T. P. Russell, R. A. J. Janssen and X. B. Peng, *J. Am. Chem. Soc.*, 2015, **137**, 7282-7285.
24. S. Chen, L. G. Xiao, X. J. Zhu, X. B. Peng, W. K. Wong and W. Y. Wong, *Chem. Commun.*, 2015, **51**, 14439-14442.
25. L. G. Xiao, S. Chen, K. Gao, X. B. Peng, F. Liu, Y. Cao, W. Y. Wong, W. K. Wong and X. J. Zhu, *ACS Appl. Mater. Inter.*, 2016, **8**, 30176-30183.
26. H. M. Qin, L. S. Li, F. Q. Guo, S. J. Su, J. B. Peng, Y. Cao and X. B. Peng, *Energy Environ. Sci.*, 2014, **7**, 1397-1401.
27. K. Gao, J. S. Miao, L. A. Xiao, W. Y. Deng, Y. Y. Kan, T. X. Liang, C. Wang, F. Huang, J. B. Peng, Y. Cao, F. Liu, T. P. Russell, H. B. Wu and X. B. Peng, *Adv. Mater.*, 2016, **28**, 4727-4733.
28. T. X. Liang, L. A. Xiao, K. Gao, W. Z. Xu, X. B. Peng and Y. Cao, *ACS Appl. Mater. Inter.*, 2017, **9**, 7131-7138.
29. G. Moran, S. Arrechea, P. de la Cruz, V. Cuesta, S. Biswas, E. Palomares, G. D. Sharma and F. Langa, *J. Mater. Chem. A.*, 2016, **4**, 11009-11022.
30. G. D. Sharma, L. Bucher, N. Desbois, E. Koukaras, C. H. Devillers, S. Biswas and C. P. Gros, *J. Mater. Chem. A.*, 2018, **6**, 8449-8461.
31. J. Kesters, P. Verstappen, M. Kelchtermans, L. Lutsen, D. Vanderzande and W. Maes, *Adv. Energy Mater.*, 2015, **5**, 1500218-1500237.
32. C. Liu, L. Zhang, L. G. Xiao, X. B. Peng and Y. Cao, *ACS Appl. Mater. Inter.*, 2016, **8**, 28225-28230.
33. R. Mishra, R. Regar, R. Singhal, P. Panini, G. D. Sharma and J. Sankar, *J. Mater. Chem. A.*, 2017, **5**, 15529-15533.
34. A. D. Zhang, C. Li, F. Yang, J. Q. Zhang, Z. H. Wang, Z. X. Wei and W. W. Li, *Angew. Chem. Int. Edit.*, 2017, **56**, 2694-2698.
35. W. T. Hadmojo, D. Yim, H. Aqoma, D. Y. Ryu, T. J. Shin, H. W. Kim, E. Hwang, W. D. Jang, I. H. Jung and S. Y. Jang, *Chem. Sci.*, 2017, **8**, 5095-5100.
36. H. D. Wang, L. G. Xiao, L. Yan, S. Chen, X. J. Zhu, X. B. Peng, X. Z. Wang, W. K. Wong and W. Y. Wong, *Chem. Sci.*, 2016, **7**, 4301-4307.
37. V. Cuesta, M. Vartanian, P. de la Cruz, R. Singhal, G. D. Sharma and F. Langa, *J. Mater. Chem. A.*, 2017, **5**, 1057-1065.
38. L. G. Xiao, T. X. Liang, K. Gao, T. Q. Lai, X. B. Chen, F. Liu, T. P. Russell, F. Huang, X. B. Peng and Y. Cao, *Acs. Appl. Mater. Inter.*, 2017, **9**, 29917-29923.
39. L. G. Xiao, K. Gao, Y. D. Zhang, X. B. Chen, L. T. Hou, Y. Cao and X. B. Peng, *J. Mater. Chem. A.*, 2016, **4**, 5288-5293.
40. L. G. Xiao, C. Liu, K. Gao, Y. J. Yan, J. B. Peng, Y. Cao and X. B. Peng, *Rsc. Adv.*, 2015, **5**, 92312-92317.
41. G. D. Sharma, G. E. Zervaki, P. Angaridis and A. G. Coutsolelos, *Rsc. Adv.*, 2014, **4**, 50819-50827.
42. Y. Matsuo, Y. Sato, T. Niinomi, I. Soga, H. Tanaka and E. Nakamura, *J. Am. Chem. Soc.*, 2009, **131**, 16048-16050.
43. W. J. Park, S. H. Chae, J. Shin, D. H. Choi and S. J. Lee, *Synthetic Met.*, 2015, **205**, 206-211.
44. J. L. Wang, Z. Wu, J. S. Miao, K. K. Liu, Z. F. Chang, R. B. Zhang, H. B. Wu and Y. Cao,

- Chem. Mater.*, 2015, **27**, 4338-4348.
45. X. F. Liu, Y. M. Sun, L. A. Perez, W. Wen, M. F. Toney, A. J. Heeger and G. C. Bazan, *J. Am. Chem. Soc.*, 2012, **134**, 20609-20612.
 46. Q. Wu, D. Deng, K. Lu and Z.-X. Wei, *Chin. Chem. Lett.*, 2017, **28**, 2065-2077.
 47. T. Lai, X. Chen, L. Xiao, L. Zhang, T. Liang, X. Peng and Y. Cao, *Chem. Commun.*, 2017, **53**, 5113-5116.
 48. S. Chen, L. Yan, L. Xiao, K. Gao, W. Tang, C. Wang, C. Zhu, X. Wang, F. Liu, X. Peng, W.-K. Wong and X. Zhu, *J. Mater. Chem. A.*, 2017, **5**, 25460-25468.
 49. T. Q. Lai, L. G. Xiao, K. Deng, T. X. Liang, X. B. Chen, X. B. Peng and Y. Cao, *ACS Appl. Mater. Inter.*, 2018, **10**, 668-675.
 50. H. Burckstummer, E. V. Tulyakova, M. Deppisch, M. R. Lenze, N. M. Kronenberg, M. Gsanger, M. Stolte, K. Meerholz and F. Wurthner, *Angew. Chem. Int. Edit.*, 2011, **50**, 11628-11632.
 51. Y. Z. Lin, L. C. Ma, Y. F. Li, Y. Q. Liu, D. B. Zhu and X. W. Zhan, *Adv. Energy Mater.*, 2013, **3**, 1166-1170.
 52. J. L. Bredas, J. E. Norton, J. Cornil and V. Coropceanu, *Accounts Chem. Res.*, 2009, **42**, 1691-1699.
 53. L. G. Xiao, H. D. Wang, K. Gao, L. S. Li, C. Liu, X. B. Peng, W. Y. Wong, W. K. Wong and X. J. Zhu, *Chem-Asian J.*, 2015, **10**, 1513-1518.
 54. L. Yuan, K. Lu, B. Z. Xia, J. Q. Zhang, Z. Wang, Z. Y. Wang, D. Deng, J. Fang, L. Y. Zhu and Z. X. Wei, *Adv. Mater.*, 2016, **28**, 5980-5985.
 55. T. E. O. Screen, K. B. Lawton, G. S. Wilson, N. Dolney, R. Ispasoiu, T. Goodson, S. J. Martin, D. D. C. Bradley and H. L. Anderson, *J. Mater. Chem.*, 2001, **11**, 312-320.
 56. Z. H. Wu, C. Sun, S. Dong, X. F. Jiang, S. P. Wu, H. B. Wu, H. L. Yip, F. Huang and Y. Cao, *J. Am. Chem. Soc.*, 2016, **138**, 2004-2013.
 57. J. Min, X. C. Jiao, V. Sgobba, B. Kan, T. Heumuller, S. Rechberger, E. Spiecker, D. M. Guldi, X. J. Wan, Y. S. Chen, H. Ade and C. J. Brabec, *Nano Energy*, 2016, **28**, 241-249.
 58. K. Gao, W. Y. Deng, L. G. Xiao, Q. Hu, Y. Y. Kan, X. B. Chen, C. Wang, F. Huang, J. B. Peng, H. B. Wu, X. B. Peng, Y. Cao, T. P. Russelle and F. Liu, *Nano Energy*, 2016, **30**, 639-648.
 59. B. Kan, Q. Zhang, M. M. Li, X. J. Wan, W. Ni, G. K. Long, Y. C. Wang, X. Yang, H. R. Feng and Y. S. Chen, *J. Am. Chem. Soc.*, 2014, **136**, 15529-15532.
 60. K. Kawashima, Y. Tamai, H. Ohkita, I. Osaka and K. Takimiya, *Nat. Commun.*, 2015, **6**, 10085-10093.
 61. H. J. Bin, Z. G. Zhang, L. Gao, S. S. Chen, L. Zhong, L. W. Xue, C. Yang and Y. F. Li, *J. Am. Chem. Soc.*, 2016, **138**, 4657-4664.
 62. J. Liu, S. S. Chen, D. P. Qian, B. Gautam, G. F. Yang, J. B. Zhao, J. Bergqvist, F. L. Zhang, W. Ma, H. Ade, O. Inganas, K. Gundogdu, F. Gao and H. Yan, *Nat. Energy*, 2016, **1**, 16089-16095.
 63. J. Zhang, K. Jiang, G. Yang, T. Ma, J. Liu, Z. Li, J. Y. L. Lai, W. Ma and H. Yan, *Adv. Energy Mater.*, 2017, 1602119.
 64. Z. Du, X. Bao, Y. Li, D. Liu, J. Wang, C. Yang, R. Wimmer, L. W. Städe, R. Yang and D. Yu, *Adv. Energy Mater.*, 2018, 1701471.
 65. D. Baran, T. Kirchartz, S. Wheeler, S. Dimitrov, M. Abdelsamie, J. Gorman, R. S. Ashraf, S. Holliday, A. Wadsworth, N. Gasparini, P. Kaienburg, H. Yan, A. Amassian, C. J. Brabec, J. R.

- Durrant and I. McCulloch, *Energy Environ. Sci.*, 2016, **9**, 3783-3793.
66. K. Sun, Z. Y. Xiao, S. R. Lu, W. Zajaczkowski, W. Pisula, E. Hanssen, J. M. White, R. M. Williamson, J. Subbiah, J. Y. Ouyang, A. B. Holmes, W. W. H. Wong and D. J. Jones, *Nat. Commun.*, 2015, **6**, 6013-6021.
67. P. W. M. Blom, V. D. Mihailetschi, L. J. A. Koster and D. E. Markov, *Adv. Mater.*, 2007, **19**, 1551-1566.
68. J. L. Wu, F. C. Chen, Y. S. Hsiao, F. C. Chien, P. L. Chen, C. H. Kuo, M. H. Huang and C. S. Hsu, *Acs. Nano.*, 2011, **5**, 959-967.
69. S. R. Cowan, A. Roy and A. J. Heeger, *Phys. Rev. B.*, 2010, **82**, 245207-245216.
70. W. L. Leong, S. R. Cowan and A. J. Heeger, *Adv. Energy Mater.*, 2011, **1**, 517-522.
71. L. J. A. Koster, V. D. Mihailetschi, R. Ramaker and P. W. M. Blom, *Appl. Phys. Lett.*, 2005, **86**, 123509-123511.
72. M. M. Mandoc, W. Veurman, L. J. A. Koster, B. de Boer and P. W. M. Blom, *Adv. Funct. Mater.*, 2007, **17**, 2167-2173.

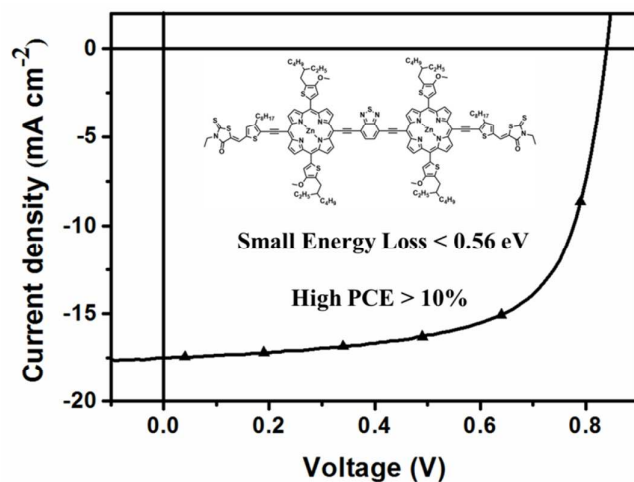


Table of contents entry

A novel dimeric porphyrin small molecule ZnP2BT-RH has been developed for OSCs with PCE more than 10%. The 10% PCE is the highest for porphyrin-based OSCs with a conventional structure, and this E_{loss} of 0.56 eV is also the smallest among the small molecule-based OSCs with a PCE higher than 10% to date. SVA treatment induces π - π stacking and tightens lamellar packing of porphyrin molecules and also improves phase purity of blend films which enhance the exciton separation and reduce the recombination.